Frontiers in Heat and Mass Transfer

Tech Science Press

https://doi.org/10.32604/fhmt.2026.079464

ARTICLE

Study on Heat Transfer in Double-Layer Topologically Optimized Microchannels under Non-Uniform Heat Sources in 2.5D Chips

Yechao Qin[1], **Zezhong Hou**[1], **Xiaojun Dai**[2], **Zhenqian Chen**[1] **and Bo Xu**[1,*]

[1]School of Energy and Environment, Southeast University, Nanjing, China
[2]Technology and Engineering Center for Space Utilization, Chinese Academy of Sciences, Beijing, China
*Corresponding Author: Bo Xu. Email: xubo@seu.edu.cn

Received: 21 January 2026; Accepted: 25 March 2026; Published: 29 June 2026

ABSTRACT: To address the increasing thermal management demands of electronic devices, this study proposes a single-inlet, single-outlet counterflow double-layer microchannel structure optimized for non-uniform heat sources and conducts a numerical analysis. The research focuses on designing a double-layer microchannel structure through topology optimization under 2.5D chip non-uniform heat source conditions. Its heat dissipation performance is compared with traditional linear microchannels to analyze the advantages of the topology-optimized microchannel. In a simulated 2.5D heat source scenario comprising a 240 W logic chip and four 40 W memory chips, the average temperature at the bottom of the topologically optimized microchannel heat sink decreased by 2 to 4 K compared to the conventional design when the inlet Reynolds number ranged from 500 to 2300. Concurrently, the system pressure drop was significantly reduced by 32% to 42%. These results demonstrate that this innovative design offers significant advantages in enhancing cooling efficiency and reducing energy consumption. Furthermore, due to its unique counter-current heat transfer mechanism, the structure also exhibits markedly improved temperature uniformity. This study provides an efficient design solution for advanced electronic thermal management scenarios characterized by constrained design space and stringent requirements for thermal stress management and integration density.

KEYWORDS: Heat exchange maximization; liquid cooled heat sink; objective function; topology optimization

1 Introduction

With the advancement of information technology and artificial intelligence, computing and memory demands have surged dramatically, driving continuous miniaturization and increased transistor integration. While three-dimensional integrated circuits offer extremely high integration density, they require stringent manufacturing processes and suffer from severe thermal concentration issues [1]. To facilitate the transition to 3D integrated circuits, 2.5D chips that integrate modules onto silicon interposers have been proposed. Their high integration density and larger heat dissipation area make them an optimal packaging solution for bridging 2D and 3D integrated circuits [2]. Nevertheless, despite these advancements, thermal management remains a critical bottleneck due to the persistent high integration density, necessitating stable and reliable cooling solutions within confined spaces. Air cooling technology has limited thermal dissipation capacity and can no longer effectively address the heat dissipation challenges of highly integrated electronic components [3]. Currently, common techniques for tackling high heat flux density include phase-change cooling [4] and liquid cooling radiators [5]. Although phase-change cooling utilizes the latent heat of vaporization for greater thermal dissipation potential, its cooling mechanism is constrained by the critical

heat flux density [6]. Single-phase liquid-cooled microchannel heat sinks have achieved extensive use owing to their superior heat transfer efficiency, straightforward and stable design, and economical nature [7]. The internal flow channel structure of microchannel heat sinks significantly determines their flow and heat transfer performance [8]. Due to the spatial limitations of chip integration, traditional microchannel structures increasingly fail to satisfy the heat management requirements of electronic devices. Consequently, researchers have begun optimizing flow channel parameters within limited spaces to achieve optimal cooling performance [9].

Since Tuckerman and Pease [10] initially introduced microchannel heat sinks, extensive research has meticulously examined their remarkable heat transfer efficiency and compact structural design [11]. To improve the heat transferring effectiveness in microchannels, scholars have performed comprehensive optimization designs on flow channel architectures, including tree-like microchannels [12] and honeycomb microchannels [13]. Simultaneously, to meet high heat flux density cooling demands, various cross-sectional shapes [14], manifold structures [15], and double-layer microchannel designs [16] have been developed. Bejan and Errera [17] subsequently proposed a construction theory and explored the generation principles of tree-like structural elements [18]. However, existing microchannel structure designs remain highly dependent on researchers' experience, exhibiting inherent limitations particularly when addressing microchannels for non-uniform heat sources. While traditional straight-through microchannel heat sinks can achieve thermal resistances of 0.1–0.5 K·cm^2/W, fluid temperature gradients can reach 30–50°C under non-uniform heating conditions. Therefore, an immediate requirement exists for a microchannel design process that can be tailored to particular heat source distributions to satisfy the increasing demand for elevated heat flux densities.

Topology optimization (TO) techniques provide novel strategies for microchannel design, overcoming the limitations of flow channel design that rely on subjective decision-making. Bendsøe and Kikuchi [19] were the first to propose a topology optimization-based method for finding optimal solutions, applying it to structural design to achieve optimal structures. Borrvall and Petersson [20] enhanced this methodology for fluid dynamics by incorporating an additional damping term—the Brinkman penalty—into the flow equations to model solid material resistance. By modifying material allocation within the design domain, guided by objective functions and constrained by boundary conditions, topology optimization efficiently generates microchannel structures with complex curved geometries. In convective heat transfer, the primary goal of topology optimization is to improve thermal transfer efficiency while minimizing pressure drop. Zhao et al. [21] utilized topology optimization to reduce flow energy dissipation. Koga et al. [22] achieved dual-objective topology optimization for microchannel convective heat transfer by defining a weighted objective function balancing heat exchange and fluid flow. Palumbo et al. [23] employed a topology optimization method based on variable density to minimize temperature nonuniformity in water-cooled microchannel heat sinks fabricated using thermal spray additive manufacturing. The optimized heat sinks exhibited lower surface temperatures and reduced temperature gradients under various flow conditions. Research findings demonstrate that channel branching increasingly intensifies with a greater emphasis on the temperature optimization target. In 1999, Vafai and Zhu [24] introduced a microchannel heat sink design with a double-layer counterflow configuration to successfully mitigate the persistent temperature increase along the flow direction in single-layer heat sinks. They observed that the dual-layer design significantly reduced temperature rise in the bottom-flow direction while delivering more uniform cooling performance. Subsequently, numerous studies based on this dual-layer concept have emerged, further enhancing microchannel heat sink performance [25]. In the existing literature, over 80% of TO microchannel studies focus on uniform heat sources, and most optimization frameworks employ constant fluid properties, neglecting the effects

of viscosity and thermal conductivity variations with temperature. Particularly for chips with actual non-uniform heat sources, these omissions may lead to performance prediction deviations as high as 15% to 25%. Furthermore, most literature has limited investigation into channels under multiple weighting factors, typically presenting only one or a few topological results without systematically screening outcomes across a wide range of weighting factors. The determination of weighting coefficients is often arbitrary, lacking scientific justification based on rigorous Pareto frontier analysis.

To enhance the thermal performance of 2.5D chips, this paper employs a topology optimization design approach combined with a counter-current flow configuration. By adjusting inlet conditions, a two-dimensional rectangular flow channel undergoes topology optimization, resulting in a dual-layer, topology-optimized microchannel structure. This configuration achieves exceptional heat dissipation performance and temperature uniformity. The locally scaled flow channel structure ensures optimal flow-to-heat load matching while expanding the heat dissipation area and enhancing cooling capacity without significantly increasing the pressure drop. The upper microchannel balances the temperature distribution of the lower microchannel, effectively reducing peak temperatures and optimizing thermal uniformity across the chip surface. This topologically optimized microchannel heat sink increases the fluid flow path length, overcoming uneven surface temperature distribution while maintaining a low pressure drop and superior thermal performance. This research offers a novel design approach for developing efficient, reliable microchannel heat sinks in confined spaces and under low-flow conditions. The design holds broad application prospects, particularly for electronic device cooling and aerospace thermal management systems.

2 Topology Optimization Model

2.1 Description of the Physics Problem

Fig. 1 illustrates the physical model of the microchannel heat sink (MCHS) examined in this study, which primarily consists of a flow channel layer and a heat source layer. The operational principle entails the working fluid arriving via the intake of the flow channel layer, flowing through the heat sink, and dissipating heat generated by the heat source layer—a 2.5D chip comprising four memory chips and one logic chip. This process achieves effective cooling and thermal management. The flow channel configuration markedly affects flow dynamics and thermal dissipation properties. An optimum design of the flow channel structure is crucial to achieve a balance between flow performance and heat dissipation capacity while maintaining a uniform temperature distribution. Considering the manufacturability of the MCHS and the convergence requirements of the topology optimization model, this study simplifies each heat dissipation flow channel layer into a two-dimensional model, as shown in the figure, with fixed inlet and outlet positions. A 2.5D heat source boundary condition is applied to the lower design domain.

The heat source is located only at the bottom of the lower microchannel; the upper microchannel does not come into direct contact with the heat source, and heat must be conducted upward through the solid structure of the lower layer and the intermediate layer. Therefore, there is a fundamental difference between the heat dissipation functions of the upper and lower microchannels: the lower layer bears the primary heat dissipation function, while the upper layer serves a supplementary role. This study employs a split-topology optimization strategy: the upper and lower layers of microchannels are optimized independently, without any coupling between them. Additionally, for the series configuration, the upper wall surface at the outlet of the lower microchannel is cooled by the upper layer, which further reduces the temperature difference on the upper wall surface of the lower microchannel compared to a single-layer microchannel. Consequently, the upper wall surface of the lower microchannel exhibits excellent temperature uniformity. At the same time, the upper layer must obtain heat through conduction, resulting in a difference in heat

dissipation contributions between the two layers. Based on system-level thermal analysis, a uniform heat source was established as the thermal boundary condition for the top-layer topological optimization.

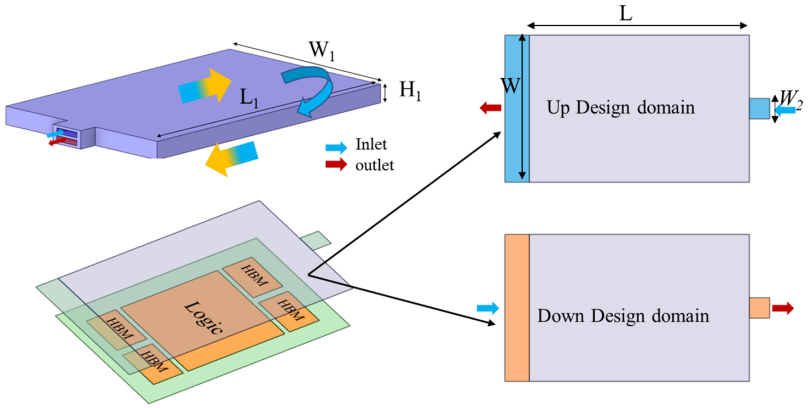

Figure 1: Schematic diagram of double-layer microchannel topology optimization.

Additionally, symmetric boundary conditions were employed during the topology optimization process to halve the computational domain and reduce computational costs, with the complete geometry obtained by mirroring.

2.2 Interpolation Function

Within defined objective functions and limitations, iterative calculations of material distribution are performed using optimization algorithms to obtain the corresponding optimal topology. A design density parameter, γ, is introduced, with values ranging from 1 (fluid material) to 0 (solid material) within each finite element cell. To achieve a clear and distinct material distribution and to avoid the adverse effects of intermediate density values on the overall distribution, a "penalty" treatment is applied to γ. The defined inverse permeability, α, is designed to reduce the occurrence of intermediate density values. This paper employs the following parametric convex interpolation function:

$$\alpha(\gamma) = \alpha_s + (\alpha_f - \alpha_s)\,\gamma \frac{1 - q_p}{\gamma + q_p} \tag{1}$$

Based on the definition of inverse permeability α in the porous medium model, and by combining α with the design variable γ through convex function interpolation, Eq. (5) can be rewritten as follows:

$$\alpha(\gamma) = \frac{\mu}{Da \cdot L^2} \cdot \frac{1 - \gamma}{q_p + \gamma} \tag{2}$$

Similarly, interpolation functions for thermal conductivity k, density ρ, and specific heat capacity c_p are provided:

$$k(\gamma) = k_s + (k_f - k_s)\,\gamma \frac{1 - q_p}{\gamma + q_p} \tag{3}$$

$$\rho(\gamma) = \rho_s + (\rho_f - \rho_s)\,\gamma \frac{1 - q_p}{\gamma + q_p} \tag{4}$$

$$c_{\mathrm{p}}(\gamma) = c_{\mathrm{p,s}} + \left(c_{\mathrm{p,f}} - c_{\mathrm{p,s}}\right)\gamma\frac{1-q_{\mathrm{p}}}{\gamma+q_{\mathrm{p}}} \tag{5}$$

where k_{s}, ρ_{s}, and $c_{\mathrm{p,s}}$ represent the thermal conductivity, density, and specific heat capacity of the solid substance.

2.3 Control Equation

Velocity and thermal analysis are crucial for clarifying the heat dissipation mechanisms in the MCHS, the following are assumptions regarding flow and heat transfer in the design domain: (1) Since the *Re* is below 2300, the fluid flow within the channel is laminar; (2) The fluid is incompressible.

The continuum equation is given by

$$\nabla \cdot \mathbf{u} = 0 \tag{6}$$

where **u** is the fluid velocity vector.

The momentum equation is given by

$$\rho_f(\mathbf{u}\cdot\nabla\mathbf{u}) = -\nabla\mathbf{p} + \mu\nabla^2\mathbf{u} + \mathbf{F} \tag{7}$$

where ρ_f is the fluid density, p is the pressure, μ is the dynamic viscosity and **F** is the volume force.

The volume force can be expressed as follows:

$$\mathbf{F} = -\alpha(\lambda)\,\mathbf{u}$$

where α is the reverse permeability of the porous medium.

In solid domain, the energy equation is given by

$$-\nabla\cdot(k_s\nabla T) = Q \tag{8}$$

In fluid domain, the energy equation is given by

$$\rho_f c_{p,f}(\mathbf{u}\cdot\nabla)\,T = kf\nabla^2 T + Q \tag{9}$$

where $c_{p,f}$ is the fluid specific heat capacity, Q is the heat source, k_s indicates the solid thermal conductivity, and k_f indicates the fluid thermal conductivity.

2.4 Filtering and Projection Methods

To mitigate inconsistencies in optimization results caused by mesh partitioning, this design approach incorporates a density filtering method based on the Helmholtz partial differential equation [26], which is expressed as follows:

$$-r_{\min}^2\nabla^2\tilde{\gamma} + \tilde{\gamma} = \gamma \tag{10}$$

where $r_{\min}$ is the defined filtering radius, serving as both the pre-filtered and post-filtered design variable. To simultaneously ensure computational accuracy and manufacturability, $r_{\min}$ is set to 0.1 mm in this study.

The filtered density reintroduces intermediate density cells, resulting in gray-scale cells within the filtered topology-optimized structure. To ensure clear fluid-solid boundaries, the hyperbolic tangent projection

method [27] is applied to project the filtered design variable, yielding a clear flow channel topology-optimized structure. The expression is as follows:

$$\widehat{\tilde{\gamma}} = \frac{\tanh\left(\beta\left(\tilde{\gamma} - \gamma_\beta\right)\right) + \tanh\left(\beta\gamma_\beta\right)}{\tanh\left(\beta\left(1 - \gamma_\beta\right)\right) + \tanh\left(\beta\gamma_\beta\right)} \tag{11}$$

here, $\widehat{\tilde{\gamma}}$ represents the projected design variable, β denotes the projection slope, and γ_β signifies the projection point. In the model studied herein, $\beta = 8$ and $\gamma_\beta = 0.5$. As shown in Fig. 2, it can be observed that under these conditions, $\widehat{\tilde{\gamma}}$ more readily approaches 0 or 1 as varies, thereby achieving a more distinct material distribution and effectively reducing the occurrence of gray-scale units.

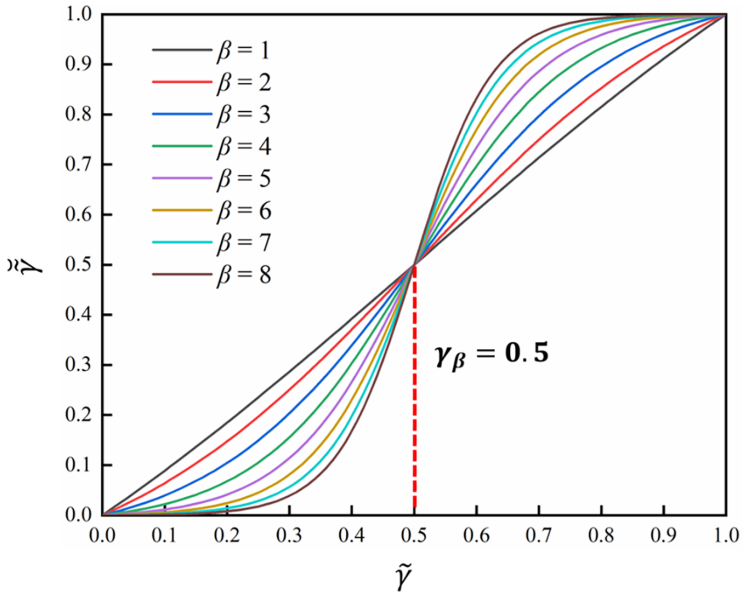

Figure 2: Projection curves under different projection slopes β.

2.5 Realization of the Target Space

The efficacy of the MCHS is often assessed by their thermal dissipation capability and hydraulic resistance. An optimal MCHS must attain superior heat dissipation while preserving low flow resistance. This work utilizes average temperature (T_{avg}) and resistance loss (Φ) to concurrently limit these two variables, quantifying thermal performance and hydraulic loss. T_{avg} offers a clear representation of the heat transfer efficiency of the MCHS. A reduced T_{avg} value under equivalent operating conditions signifies enhanced system-level thermal efficiency. The Φ directly denotes the mechanical energy loss attributable to viscous friction in the flow channels [28]. An elevated Φ value necessitates increased pumping power to sustain fluid flow, thereby augmenting total energy consumption. The methodologies for calculating T_{avg} and Φ are explained below:

$$\Gamma = \frac{1}{A}\int_\Omega T d\Omega \tag{12}$$

$$\Phi = \frac{1}{2}\mu\int_\Omega \nabla \mathrm{u}\cdot\nabla \mathrm{u} d\Omega + \int_\Omega \alpha(\gamma)\,\mathrm{u}\cdot\mathrm{u} d\Omega \tag{13}$$

To enable the resolution, the multi-objective optimization issue must be converted into a single-objective optimization problem appropriate for numerical techniques. The original multi-objective function is specifically transformed into a weighted sum, and the objective functions for temperature and pressure drop are nondimensionalized. Due to significant differences in the magnitude of the dimensionless objective function values, the objective function for topology optimization is expressed using logarithmic notation:

$$\Phi^* = \frac{\Phi}{\overline{\Phi}}; \Gamma^* = \frac{\Gamma}{\overline{\Gamma}} \tag{14}$$

$$\Psi(\gamma) = w_1 \ln\left(\frac{\Phi}{\overline{\Phi}}\right) + w_2 \ln\left(\frac{\Gamma}{\overline{\Gamma}}\right) \tag{15}$$

where w_1 is the flow enhancement weighting factor; w_2 is the heat dissipation enhancement weighting factor, $\overline{\Phi}$ is the baseline flow dissipation in the initial domain; $\overline{\Gamma}$ is the baseline temperature in the initial domain. Due to the differing sensitivities of the objective function to temperature and pressure drop, and because the flow channel design prioritizes reducing the average temperature, the weighting coefficient for temperature is placed in the denominator. A topology optimization method with weighting coefficients $w > 1$ is employed for microchannel design to achieve a flow channel structure with superior heat dissipation performance. The weighting factor w is defined by the following objective function:

$$w = \frac{w_2}{w_1} \tag{16}$$

This study employs the Method of Moving Asymptotes (MMA) [29], with a maximum iteration count set to 400 and an optimization tolerance of 10^{-8}. Under the boundary and constraint conditions investigated, stable and reliable topology optimization results are consistently obtained.

3 3D Assessment

3.1 3D Numerical Model

To assess the outcomes of two-dimensional topology optimization, where white areas denote solid fins and black areas signify fluid, the contour line corresponding to $\gamma = 0.5$ is retrieved to delineate the fluid-solid interface. The contour line is subsequently stretched in the z-direction to create the entire three-dimensional structure, as depicted in Fig. 3 [30–32].

Table 1 presents the initial boundary conditions and geometric dimensions of the design domain used in the topology optimization model. The logic chip measures 26 mm × 26 mm and contains heat source *Q1*. Each of the four memory modules measures 8 mm × 12 mm and contains heat source *Q2*. Water is used as the working fluid (fluid domain), while copper is selected as the heat dissipation material (solid domain). Due to significant temperature-dependent variations in fluid properties—particularly the high sensitivity of viscosity to temperature—calculations of flow losses using non-actual physical parameters would produce results that deviate substantially from reality. To better approximate actual operating conditions and avoid compromising the final results of the topology optimization [33], this study employs the following equation to describe the temperature-dependent variation of fluid properties [34]:

$$\rho = a_\rho + b_\rho T_C + c_\rho T_C^2 + d_\rho T_C^{2.5} + e_\rho T_C^3 \tag{17}$$

$$\mu = \frac{1}{a_\mu + b_\mu T_C + c_\mu T_C^2 + d_\mu T_C^3} \tag{18}$$

$$c_{p,f} = a_{C_P} + b_{C_P} T_C + c_{C_P} T_C^{1.5} + d_{C_P} T_C^2 + e_{C_P} T_C^{2.5} \tag{19}$$

$$k_f = a_k + b_k T_C + c_k T_C^{1.5} + d_k T_C^2 + e_k T_C^{0.5} \tag{20}$$

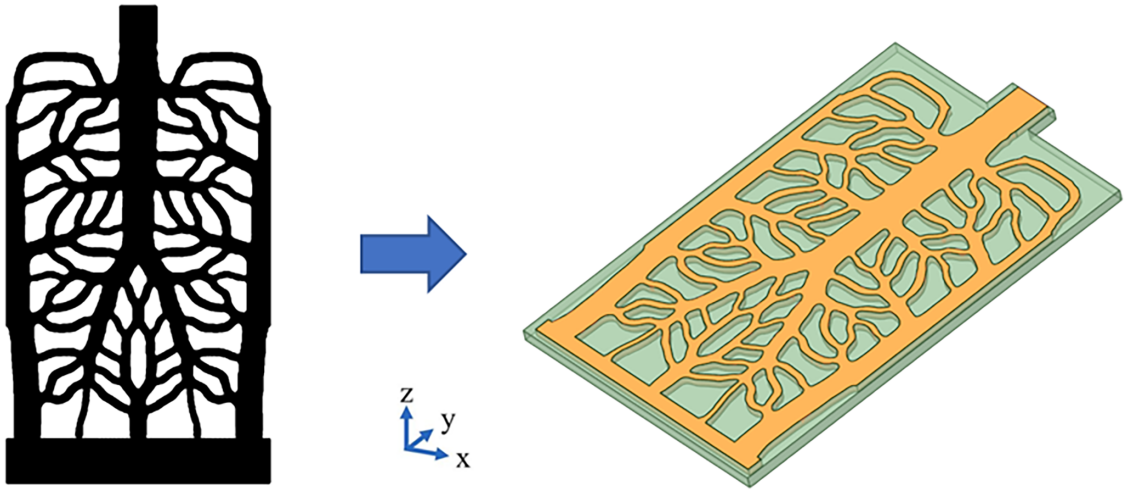

Figure 3: Three-dimensional microchannel fabrication process.

Table 1: Preliminary parameters for topology optimization models.

Parameters	Value	Unit
Lower layer inlet velocity v_2	0.05	m/s
Upper layer inlet velocity v_1	0.01	m/s
Inlet temperature T_{in}	293.15	K
Ambient temperature T_0	293.15	K
Darcy Number Da	10^{-4}	/
Weighting factor w	10–90	/
Radius of the inner circle r_{mesh}	0.1	mm
Volume fraction φ	0.4~0.7	/
Penalty factor p	0.1	/
Outlet pressure P_{out}	0	Pa
Topology domain dimensions L, W	54, 36	mm
MCHS structure dimensions L_1, W_1, H_1	58, 38, 3.5	mm
MCHS Single-Layer Height H	1	mm
MCHS Partition Thickness L_2	0.5	mm
MCHS Inlet/Outlet Width W_2	5	mm
Non-Uniform Heat Sources $Q1$, $Q2$	240, 40	W

$T_C = T_K - 273.15$ K, where T_K denotes the temperature in Kelvin; the coefficients used in the above equation are presented in Table 2:

Table 2: Polynomial coefficients.

	a	*b*	*c*	*d*	*e*
ρ	999.8	0.06832	−0.01074	0.0008214	$-2.303 * 10^{-5}$
μ	557.8	19.41	0.1360	$-3.116 * 10^{-4}$	
$c_{p,f}$	4217	−5.618	1.299	−0.1154	$4.150 * 10^{-3}$
k_f	0.5650	0.002636	−0.0001252	$-1.515 * 10^{-6}$	−0.0009413

Based on the multi-objective optimization parameters and initial conditions derived from the above topology optimization, the following underlying microchannel topology results were generated in Table 3:

Table 3: TO-generated MCHS under various circumstances.

	φ = 0.4	φ = 0.5	φ = 0.6	φ = 0.7
w = 10				
w = 20				
w = 30				
w = 40				
w = 50	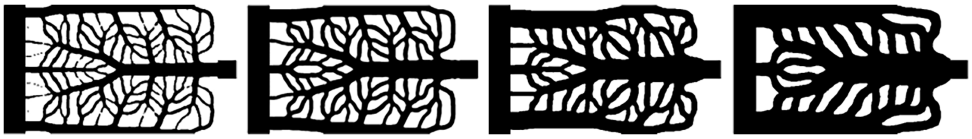			
w = 60				
w = 70	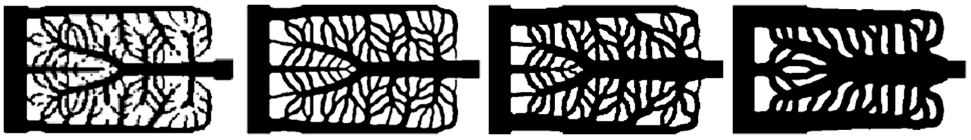			

(Continued)

Table 3 (continued)

	φ = 0.4	φ = 0.5	φ = 0.6	φ = 0.7
w = 80				
w = 90				

As shown in Fig. 4, a series of Pareto-optimal design schemes were obtained by adjusting the weighting factor w from 10 to 90. As the value of w increases, the design schemes progressively shift toward optimizing the temperature objective function. Although flow performance declines, the decrease is relatively gradual and remains within an acceptable range throughout. This demonstrates that the weighting factor can effectively regulate design bias while avoiding the introduction of critical thresholds that cause abrupt changes in the results.

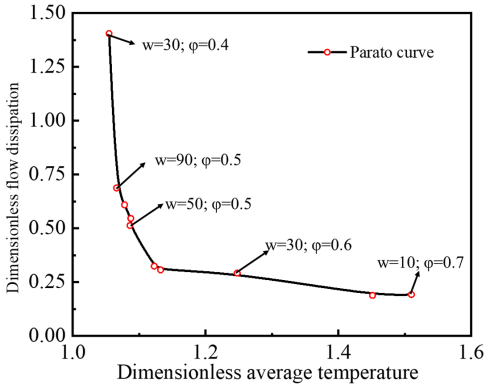

Figure 4: Pareto optimality curve.

3.2 Grid Independence Check

This paper selects a topology-optimized radiator with constraints w = 50 and φ = 0.5 to perform grid independence verification. Table 4 presents simulation data for the lower microchannel at Re = 1400 under different mesh resolutions, where errors are calculated according to Eq. (21), utilizing Mesh 6 of the highest quality mesh as the J_a. Table 4 illustrates that the discrepancies between Mesh 4 and Mesh 6 for inlet-outlet pressure (ΔP) and T_{avg} difference are both within 1%. Given considerations of computational precision and expense, using grid 4 as the simulation model, proceed with the subsequent simulation work.

$$e\% = \left| \frac{J_b - J_a}{J_a} \right| \times 100\% \tag{21}$$

Table 4: Verification of grid independence.

	Mesh Numbers	Δ *P*/Pa	e_1/%	T_{avg}/K	e_1/%
Mesh 1	405,368	2106.24	19.540%	311.55	−3.730%
Mesh 2	812,635	1908.96	8.343%	316.58	−2.175%
Mesh 3	1,635,672	1960.05	11.243%	318.59	−1.554%
Mesh 4	2,435,961	1746.59	−0.872%	322.77	−0.263%
Mesh 5	3,250,949	1812.36	2.860%	322.97	−0.201%
Mesh 6	4,876,339	1761.96	–	323.62	–

3.3 Data Processing

(1) Evaluation metrics for thermal performance

In the research, we employ temperature standard deviation (T_δ) and T_{avg} to thoroughly assess the heat transfer efficiency of microchannels with different configurations. The equations for T_δ and T_{avg} are shown below:

$$T_{\text{avg}} = \frac{1}{A_\Omega} \int_\Omega T dA \tag{22}$$

$$T_\delta = \sqrt{\frac{1}{A_\Omega} \int_\Omega \left(T - T_{\text{avg}} \right)^2 \mathrm{d}A} \tag{23}$$

This study determines the effective heating power by utilizing the enthalpy variation between the fluid inlet and output, due to heat loss, while calculating the amount of heat generated directly by the porcelain heating pad. The precise formula is as follows:

$$Q = q_m c_{p,f} \left(T_{out} - T_{in} \right) \tag{24}$$

the mass flow rate, represented as q_m and $T_{in} - T_{out}$ indicates the temperature difference between the inlet and outlet of the MCHS.

The mean heat transfer coefficient is given by:

$$h_{\text{avg}} = \frac{Q}{A_h \left(T_{\text{avg}} - T_f \right)} \tag{25}$$

$$T_f = \frac{\Delta T_{out} - \Delta T_{in}}{In \left(\Delta T_{out} / \Delta T_{in} \right)} \tag{26}$$

$$\mathrm{Nu} = \frac{h_{\text{avg}} \cdot D_{h1}}{\lambda_f} \tag{27}$$

where A_h represents the cooling region area of the MCHS.

(2) Performance evaluation indicator for fluidity

The flow performance of the MCHS can be evaluated by measuring the pressure drop ΔP and the Re within the microchannel:

$$\Delta P = P_{in} - P_{out} \tag{28}$$

$$Re = \frac{\rho u D_{h2}}{\mu} \tag{29}$$

$$D_{h2} = \frac{4A_w}{P_w} \tag{30}$$

where A_w represents the cross-sectional area of the MCHS, P_w denotes the wet perimeter of the channel, and D_{h2} represents the inlet hydraulic diameter.

3.4 Model Validation

Mo et al. [35] experimentally investigated the flow and heat transfer characteristics of microchannels under laminar flow conditions. The microchannel studied is shown in Fig. 5a and features a fluid domain inlet length of 5 mm, a total length of 120 mm, a width of 60 mm, a height of 2 mm, and adjacent wall thicknesses of 1 mm. A uniform heat flux density of q_0 = 7000 W/m^2 was applied to the bottom of the liquid cooling plate. Nine K-type thermocouples were arranged on the upper wall surface (Fig. 5b). The numerical model in this study was validated by simulating this experiment. The working fluid was water with an inlet temperature of 293.15 K. Table 5 presents comparisons between numerical results and experimental data for different inlet flow rates. As the inlet flow rate increases, the trends in average temperature and ΔP at the bottom of the MCHS in the three-dimensional model align with the experimental findings.

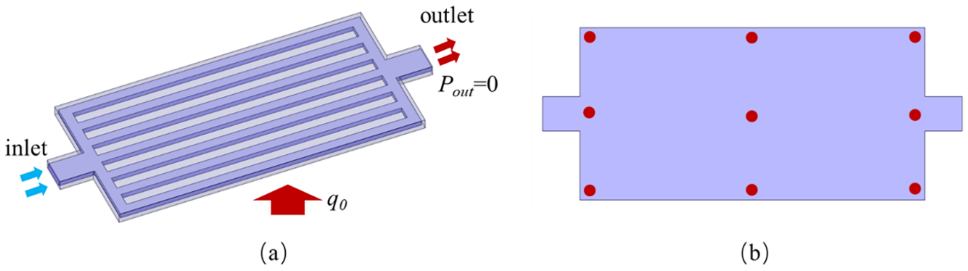

Figure 5: Experimental study of a linear microchannel by Mo et al. (**a**) Diagram of the experimental model, (**b**) Schematic diagram of temperature measurement point locations.

Table 5: Comparison and validation of Mo et al.'s experimental results with the simulation model presented in this paper.

Flow Rate (m^3/s)	Average Temperature(°C)		Error (%)	Pressure Drop (Pa)		Error (%)
	Experimental [35]	Numerical		Experimental [35]	Numerical	
7.111×10^{-6}	23.04	23.81	3.34	450.2	429.5	4.60
1.044×10^{-5}	22.31	23.08	3.47	867.33	801.2	7.62
1.389×10^{-5}	21.81	22.63	3.76	1408.9	1307.9	7.17

4 Results and Discussion

4.1 Double-Layer Topology Optimization MCHS Result Model

As shown in Fig. 6, a microchannel with a weighting factor w = 50 and a volume fraction φ = 0.5 was selected as the lower microchannel layer based on the Pareto curve in Fig. 4. This was compared with a straight-line structure having identical channel thickness and width dimensions (linear microchannel volume fraction: 0.5 ± 0.05). Simultaneously, due to the lower heat dissipation of the upper microchannel and the smaller temperature difference on the upper wall surface of the lower microchannel, the upper microchannel was topologically optimized under the constraints of weighting factor w = 50 and volume fraction φ = 0.5, based on the parameters in Table 1, under a uniform heat source of 100 W. The minimum dimensions of the topologically optimized microchannel flow channels selected during the screening process exceed 0.5 mm, ensuring their manufacturability and feasibility for application in future experiments. To evaluate the performance of the topologically optimized design, the two-dimensional models of the stretched double-layer topologically optimized microchannel and the double-layer linear microchannel were converted into three-dimensional microchannels. A comparative analysis of their heat dissipation performance was then conducted.

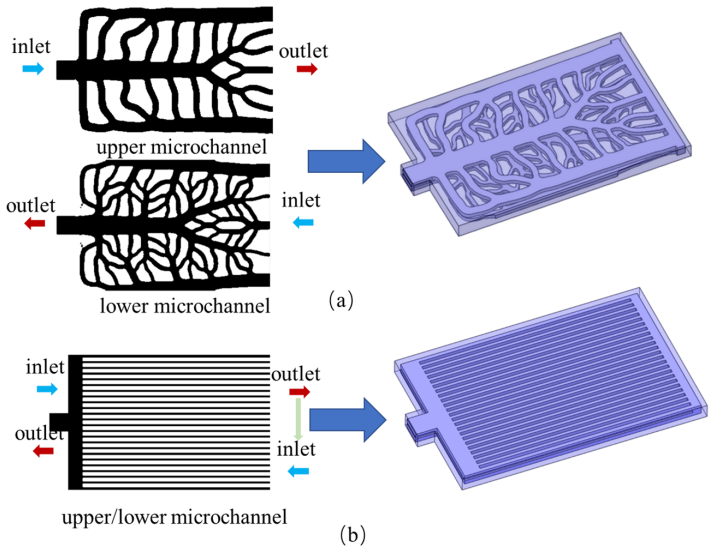

Figure 6: Double-layer microchannel model. (**a**) TO microchannel, (**b**) linear microchannel.

This study employs the commercial software Fluent 2024 to perform coupled flow and heat transfer simulations in microchannels, utilizing its built-in k-ε turbulence model for flow analysis.

4.2 Thermal Performance Analysis of Microchannel

Fig. 7 shows the T_{avg} across different MCHS structures with the *Re* under a given non-uniform heat source condition. The findings illustrate that T_{avg} decreases with increasing *Re*, though at a progressively slower rate. When the *Re* reaches 2300, the T_{avg} of the linear double-layer microchannel progressively declines, ultimately reaching 42.65°C. Notably, compared to the linear microchannel, the topologically optimized double-layer microchannel exhibits a more pronounced decrease in T_{avg}, reaching a minimum value of 40.03°C.

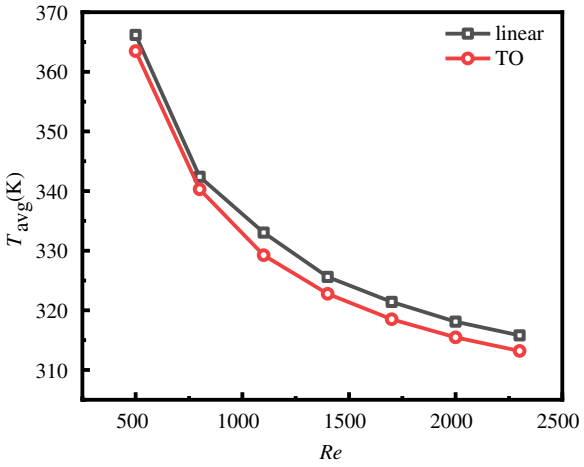

Figure 7: Relationship between T_{avg} and *Re* at the bottom of the MCHS.

Fig. 8 illustrates the temperature distribution patterns of two double-layer microchannel structures under a *Re* of 1400 conditions. Due to the combined effects of the increased Reynolds number and microchannel geometry, distinct temperature distribution patterns emerge. The temperature distribution within the channel reveals that the complex branching flow paths in the TO structure continuously disrupt the formation of the thermal boundary layer. Thinner thermal boundary layers correspond to higher heat transfer coefficients; in contrast, the boundary layer gradually thickens in straight-through channels, leading to reduced heat transfer performance downstream (the enlarged area on the right in Fig. 8d). Simultaneously, the topologically optimized design guides localized fluid deflection, enabling rapid mixing between high-temperature and low-temperature fluid regions (the enlarged area in Fig. 8a). This not only enhances heat transfer efficiency but also promotes the transport of cold fluid from the channel core toward the heated wall surface, thereby reducing surface temperature gradients. In the linear double-layer microchannel, the low-temperature zone is concentrated at the inlet of the bottom flow channel (the enlarged area on the left in Fig. 8d). In contrast, the topologically optimized microchannel exhibits a more uniform distribution of the lowest temperatures along both sides of the microchannel bottom. This discovery corresponds with the essential physical principles governing heat transfer and flow properties in these structures (refer to Fig. 9). The temperature distribution maps distinctly illustrate the respective cooling efficiencies and temperature uniformity. Compared to the linear double-layer microchannel, the topology-optimized (TO) double-layer microchannel exhibits significantly lower peak temperatures and more uniform thermal gradients. The results quantitatively align with the changes in T_{avg} and T_{δ} illustrated in Figs. 7 and 10, thus reinforcing the enhanced thermal management efficacy of the topology-optimized microchannel design under elevated heat flux conditions. Further analysis indicates that when the *Re* increases from 500 to 1400, the average temperature (T_{avg}) on the bottom wall surfaces of the TO and linear double-layer microchannels decreases by 40.77°C and 39.57°C, respectively. As *Re* increases from 1400 to 2300, the temperature reduction rates significantly diminish to 9.59°C and 8.8°C, respectively, while the T_{δ} variation remained within 0.2°C. This indicates that beyond the critical flow rate, increasing the Reynolds number only marginally enhances cooling efficiency without further improving temperature uniformity. The above results indicate that, in practical applications, selecting the appropriate microchannel based on the actual operating range is essential to maximize the heat dissipation performance [36].

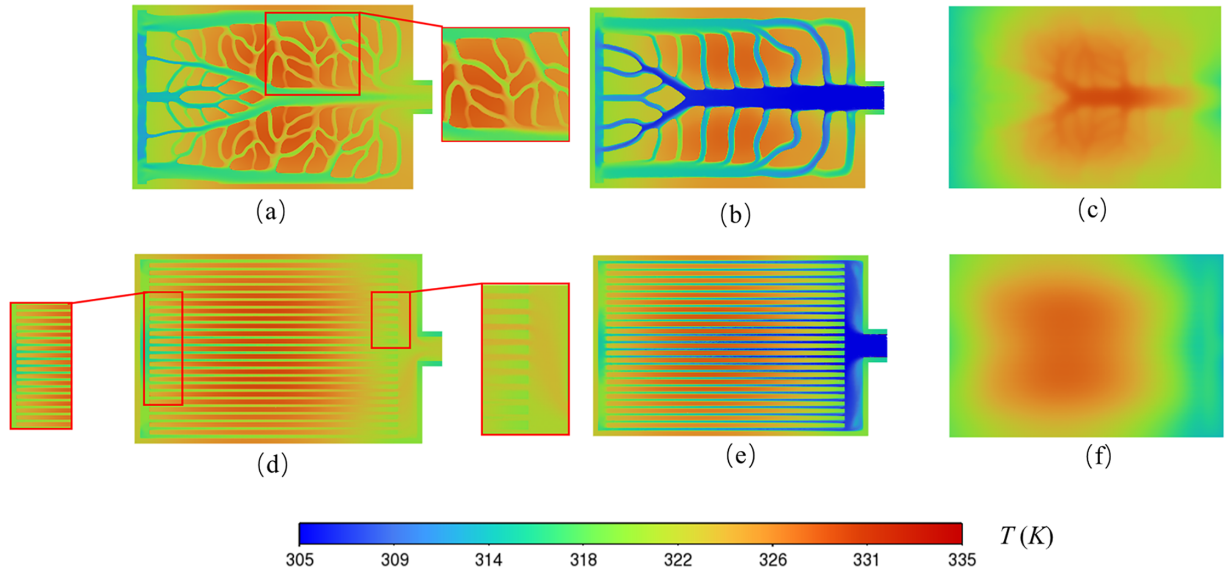

Figure 8: Temperature distribution at the bottom and intermediate interfaces of microchannels on each layer of MCHS at a Re of 1400. (**a**) TO-lower Intermediate interfaces, (**b**) TO-upper Intermediate Interfaces, (**c**) TO bottom Interfaces, (**d**) linear-lower intermediate interfaces. (**e**) linear-upper intermediate interfaces, (**f**) linear bottom Interfaces.

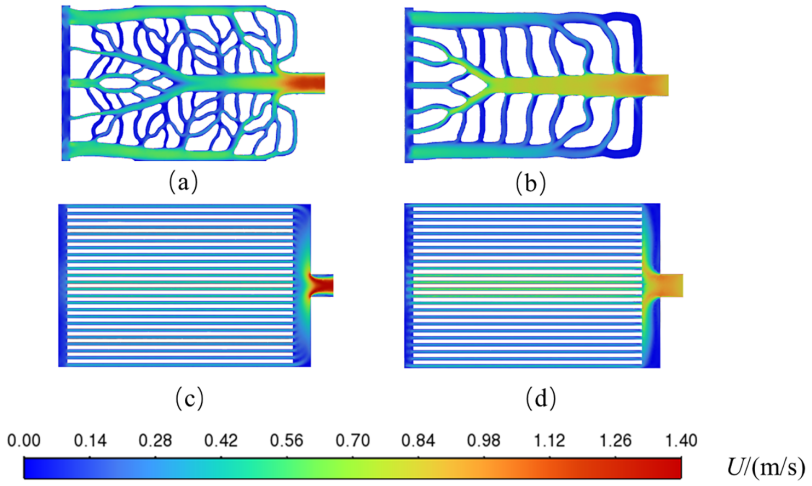

Figure 9: Velocity distribution at the mid-section of each layer in the MCHS at a *Re* of 1400. (**a**) TO-lower Intermediate interfaces, (**b**) TO-upper Intermediate interfaces, (**c**) linear-lower Intermediate interfaces, (**d**) linear-upper Intermediate interfaces.

Fig. 10 shows the T_δ across each microchannel. Superior thermal uniformity not only indirectly reflects the radiator's outstanding heat dissipation performance but also effectively reduces thermal stress on the chip, providing valuable reference for future chip applications. The topologically optimized double-layer microchannel consistently exhibits a lower temperature standard deviation, demonstrating superior temperature uniformity. In contrast, the linear double-layer microchannel shows poorer temperature uniformity. Although its uniform flow channel geometry allows fluid to flow evenly through the microchannel, the fluid distribution within the microchannel remains uneven. Consequently, this uneven flow distribution leads to

localized temperature variations [37]. These results indicate that optimizing microchannel branch designs requires balancing the microchannel structure with the uniformity of fluid velocity distribution.

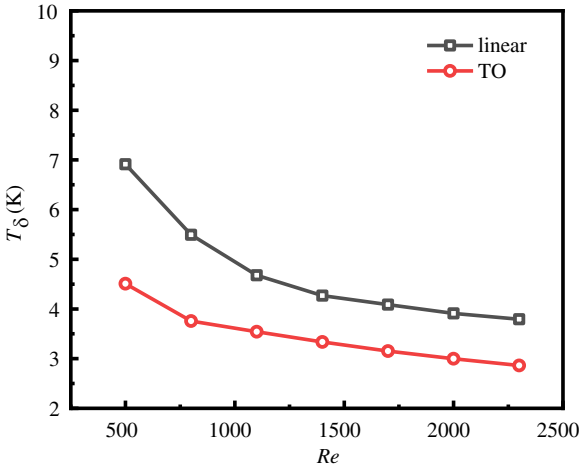

Figure 10: Standard deviation of temperature as a function of *Re*.

4.3 Characteristics of Liquid Flow in Microchannels

When the flow rate is constant, the MCHS with higher pressure drops also require greater pumping power. Therefore, in designing microchannels, it is essential to consider not only their heat dissipation capacity but also the increased power consumption resulting from elevated pressure drops. Fig. 11 illustrates the trend of ΔP as the Reynolds number increases. As the Reynolds number rises, the ΔP of different double-layer microchannels increases at an accelerating rate.

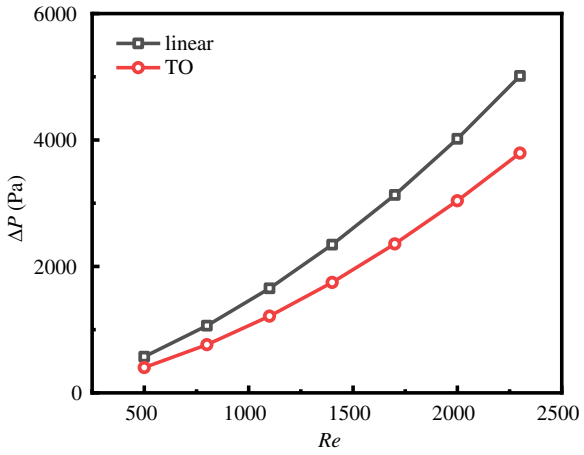

Figure 11: Pressure decline as a function of Reynolds number.

A quantitative analysis of this increase reveals that when the Reynolds number rises from 500 to 1400, the ΔP for the Topology Optimization structure and the linear structure increases by 1346 and 1774 Pa, respectively. When the Reynolds number increased to 2300, the additional pressure drop for the two microchannel structures rose to 2046 and 2668 Pa, respectively. These results demonstrate a gradual upward trend in pressure drop with increasing *Re*. The findings indicate that higher inlet coolant flow velocities lead

to greater flow resistance losses and a more rapid increase in ΔP. This phenomenon highlights the substantial influence of fluid velocity on the flow resistance of the MCHS constructions.

Since the heat transfer process in microchannels is significantly influenced by the fluid flow path and mixing degree within the channel [38], investigating the flow field distribution within microchannels is crucial. This facilitates enhancing the heat transfer efficiency of microchannels by leveraging fundamental principles of heat transfer.

Fig. 9 compares the velocity field distributions within the double-layer topologically optimized microchannel and the linear double-layer microchannel at Re = 1400, further clarifying the process underlying the improved heat transfer in the topologically optimized microchannel. The velocity field within the topologically optimized (TO) flow channel exhibits distinct velocity peaks near the inlet, outlet and central region. Combined with the temperature distribution zones in the microchannel shown in Fig. 8, it is evident that heat transfer is enhanced near high-velocity flow regions, resulting in lower temperatures. The thermal-fluid coupling analysis verifies that the TO structure facilitates effective heat dissipation while preserving uniform temperature gradients through the optimization of flow acceleration in essential areas.

Fig. 9c,d demonstrates that the coolant follows almost linear streamlines in the linear double-layer microchannel, resulting in inadequate mixing efficiency. The fluid primarily exits the central flow channel at a relatively high velocity, hence diminishing heat dissipation efficiency. Therefore, longer flow paths must be designed in high-velocity regions to enhance heat removal capacity. Fig. 9a,b shows the fluid flow paths within the topologically optimized double-layer microchannel. This optimized microchannel incorporates extended flow channels in the heat source region, ensuring that high-velocity flow is maintained throughout. Consequently, its heat transfer performance surpasses that of straight channels while providing superior temperature uniformity. Although linear microchannels exhibit higher flow velocities in the central region, the fluid exits without sufficient heat exchange with the microchannel walls, resulting in inferior heat dissipation. In summary, enhancing the heat dissipation capability of microchannels requires consideration not only of flow uniformity but also of fluid velocity within the flow path, as well as the length of high-velocity flow paths and the heat exchange area.

Fig. 12 shows the flow field distribution within the TO MCHS at Reynolds numbers of 500 and 1400. As the inlet velocity increases, a distinct velocity deflection occurs within the channel, leading to vortex formation at the branch point. This explains why viscous dissipation increases rapidly with rising flow velocity. Furthermore, the stagnation zones created by vortex formation prevent adequate mixing in adjacent regions. Consequently, simply increasing the flow velocity has a limited effect on enhancing the thermal performance of the MCHS, revealing one reason why the improvement in thermal performance diminishes as the Reynolds number increases.

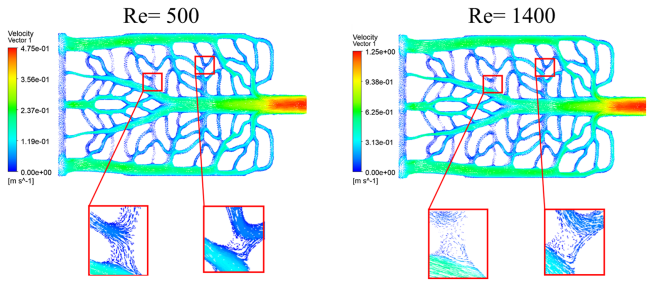

Figure 12: Flow field distribution in the intermediate section of the lower microchannel within a TO double-layer microchannel. (**a**) Flow field at an inlet Reynolds number of 500, (**b**) Flow field at an inlet Reynolds number of 900.

4.4 Evaluation of MCHS Overall Performance

To evaluate the performance advantages of the double-layer topologically optimized microchannel compared to the double-layer linear microchannel, the removal effect of topological optimization on the designed microchannel was comprehensively assessed using the relationship between pressure drop and heat transfer coefficient (expressed as $(Nu/Nu_0)/(\Delta P/\Delta P_0)^{1}/^{3}$) [39]. Here, ΔP_0 and Nu_0 represent the pressure drop and Nu of the linear double-layer MCHS, respectively. All structural data are illustrated in Fig. 13. The statistics reveal that the TO design exhibits enhanced overall heat dissipation performance. Combined with the performance of the topologically optimized microchannel in temperature uniformity, this demonstrates the broad prospects of topology optimization in heat dissipation applications.

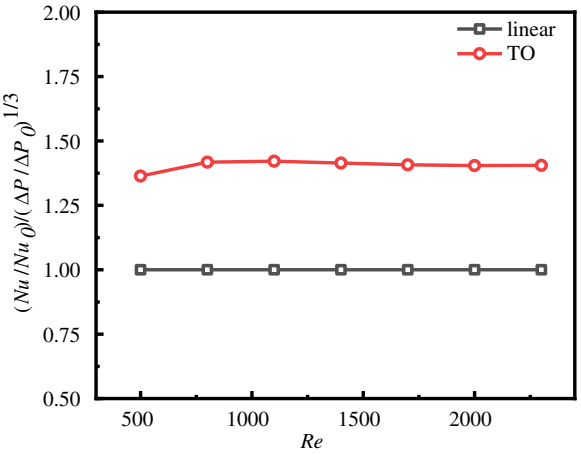

Figure 13: Overall performance results of microchannels.

5 Conclusions

To address the increasing thermal flux density demands of electronic chips, this study employs topology optimization to improve the design of the MCHS. A double-layer, topologically optimized microchannel with a microchannel φ = 0.5 and a w of 50 per layer was designed. The heat dissipation performance and pressure drop of the topologically optimized microchannels were compared with those of a conventional linear double-layer microchannel to evaluate their effectiveness in heat dissipation. Based on numerical simulation results, the following main conclusions were drawn:

(1) The quantity of branches, width, and flow channel distribution in microchannels substantially affect their heat transmission efficiency. The complex branching flow channels of the TO structure continuously disrupt the development of the thermal boundary layer. A thinner thermal boundary layer corresponds to a higher heat transfer coefficient; whereas in straight flow channels, the boundary layer progressively thickens, leading to diminished heat transfer performance downstream. Simultaneously, the topologically optimized design induces localized fluid deflection, promoting the transport of cold fluid from the channel's core region toward the heated wall surface, thereby reducing the surface temperature gradient. In the evaluated design, when the inlet Reynolds number varied from 500 to 2300, the TO double-layer microchannel demonstrated superior temperature uniformity compared to the linear microchannel. Additionally, the TO double-layer microchannel exhibited better cooling capability than the linear double-layer microchannel, achieving a temperature reduction of 2 to 4 K compared to conventional microchannels.

(2) Under identical inlet Reynolds number conditions, the smooth transition design at the branch points of the TO microchannel flow path significantly reduces pressure drop. Straight microchannels typically feature sharp right angles at branch points, leading to flow separation and vortex formation. This consumes significant energy, resulting in a substantial increase in local resistance. Within the Reynolds number range of 500 to 2300, the TO microchannel exhibits a 32% to 42% lower pressure drop compared to linear microchannels, demonstrating superior performance. Furthermore, as the Reynolds number increases, the rate of pressure drop increase in the TO microchannel is lower than that in linear microchannels.

(3) By comparing our previous research on single-layer, topologically optimized microchannels under uniform heat source conditions [40], this paper analyzes the temperature uniformity of double-layer microchannels under non-uniform heat source scenarios. The results indicate that the temperature uniformity of double-layer microchannels outperforms that of single-layer microchannels, primarily due to significantly increased heat dissipation pathways and counter-current loops. Consequently, double-layer microchannels are more suitable for chip applications requiring low cooling flow rates, high thermal stress tolerance, and high integration density.

Acknowledgement: This work was supported by the National Natural Science Foundation of China (Grant No. 52376049). We thank the Big Data Center of Southeast University for providing the facility support on the numerical calculations in this paper.

Funding Statement: This work was supported by the National Natural Science Foundation of China (Grant No. 52376049).

Author Contributions: Yechao Qin: formal analysis, investigation, methodology, writing—original draft. Zezhong Hou: conceptualization, data curation, methodology, validation. Xiaojun Dai: methodology, supervision, writing—review & editing. Zhenqian Chen: supervision, resources. Bo Xu: funding acquisition, project administration, supervision, writing—review & editing. All authors reviewed and approved the final version of the manuscript.

Availability of Data and Materials: Data will be made available on request.

Ethics Approval: Not applicable.

Conflicts of Interest: The authors declare no conflicts of interest.

Nomenclature

A_h	The cooling region area
A_w	Channel wetted cross-sectional area [m^2]
$c_{p,f}$	Fluid constant-pressure specific heat [J kg^{-1} K^{-1}]
d	Hydraulic diameter [m]
Da	Darcy number
D_{h1}	Characteristic length [m]
D_{h2}	Inlet hydraulic diameter [m]
h	Heat transfer coefficient [W m^{-2} K^{-1}]
k_s	Solid thermal conductivity
kf	Fluid thermal conductivity
Nu	Nusselt number
P	Pressure [Pa]
q''	Heat flux [W m^{-2}]
q_m	Mass flow rate [kg s^{-1}]
Q_v	Volumetric flow rate [L min^{-1}]

r Radius of the inner circle [m]
Re Reynolds number
T Temperature [K]
u Velocity [m s^{-1}]
z Coordinate in z-direction

Greek Symbols

w Weighting factor
φ Volume fraction
Ω Design domain
δ Standard deviation
μ Dynamic viscosity [Pa s]
ρ Density [kg m^{-3}]

Subscripts

avg Average
f Fluid
in Inlet
out Outlet
s Solid

References

1. Wang Z, Dong R, Ye R, Singh SSK, Wu S, Chen C. A review of thermal performance of 3D stacked chips. Int J Heat Mass Transf. 2024;235:126212. doi:10.1016/j.ijheatmasstransfer.2024.126212.
2. Abrams NC, Cheng Q, Glick M, Jezzini M, Morrissey P, O'Brien P, et al. Silicon photonic 2.5D multi-chip module transceiver for high-performance data centers. J Light Technol. 2020;38(13):3346–57. doi:10.1109/JLT.2020.2967235.
3. Ramos-Alvarado B, Bucci M. Special issue: recent advances in liquid-cooled heat sinks. Appl Therm Eng. 2024;242:122686. doi:10.1016/j.applthermaleng.2024.122686.
4. Kandlikar SG. Fundamental issues related to flow boiling in minichannels and microchannels. Exp Therm Fluid Sci. 2002;26(2–4):389–407. doi:10.1016/S0894-1777(02)00150-4.
5. Lorenzini M, Morini GL. Single-phase laminar forced convection in microchannels with rounded corners. Heat Transf Eng. 2011;32(13–14):1108–16. doi:10.1080/01457632.2011.562457.
6. Bergles AE, Kandlikar SG. On the nature of critical heat flux in microchannels. In: Proceedings of the Electronic and Photonic Packaging, Electrical Systems and Photonic Design, and Nanotechnology; 2003 Nov 15–21; Washington, DC, USA. doi:10.1115/imece2003-42383.
7. Zhang HY, Pinjala D, Wong TN, Toh KC, Joshi YK. Single-phase liquid cooled microchannel heat sink for electronic packages. Appl Therm Eng. 2005;25(10):1472–87. doi:10.1016/j.applthermaleng.2004.09.014.
8. Huang S, Zhao J, Gong L, Duan X. Thermal performance and structure optimization for slotted microchannel heat sink. Appl Therm Eng. 2017;115(3):1266–76. doi:10.1016/j.applthermaleng.2016.09.131.
9. Shi X, Li S, Mu Y, Yin B. Geometry parameters optimization for a microchannel heat sink with secondary flow channel. Int Commun Heat Mass Transf. 2019;104(5):89–100. doi:10.1016/j.icheatmasstransfer.2019.03.009.
10. Tuckerman DB, Pease RFW. High-performance heat sinking for VLSI. IEEE Electron Device Lett. 1981;2(5):126–9. doi:10.1109/edl.1981.25367.
11. Zhang X, Ji Z, Wang J, Lv X. Research progress on structural optimization design of microchannel heat sinks applied to electronic devices. Appl Therm Eng. 2023;235(1):121294. doi:10.1016/j.applthermaleng.2023.121294.
12. Zhu JF, Li XY, Wang SL, Yang YR, Wang XD. Performance comparison of wavy microchannel heat sinks with wavy bottom rib and side rib designs. Int J Therm Sci. 2019;146:106068. doi:10.1016/j.ijthermalsci.2019.106068.

13. Ghaedamini H, Salimpour MR, Mujumdar AS. The effect of svelteness on the bifurcation angles role in pressure drop and flow uniformity of tree-shaped microchannels. Appl Therm Eng. 2011;31(5):708–16. doi:10.1016/j.applthermaleng.2010.10.005.
14. Ghadami S, Kowsari-Esfahan R, Saidi MS, Firoozbakhsh K. Spiral microchannel with stair-like cross section for size-based particle separation. Microfluid Nanofluid. 2017;21(7):115. doi:10.1007/s10404-017-1950-3.
15. Pan Y, Zhao R, Nian Y, Cheng W. Study on the flow and heat transfer characteristics of pin-fin manifold microchannel heat sink. Int J Heat Mass Transf. 2022;183(11):122052. doi:10.1016/j.ijheatmasstransfer.2021.122052.
16. Patel N, Mehta HB. Experimental investigations on a variable channel width double layered minichannel heat sink. Int J Heat Mass Transf. 2021;165(11):120633. doi:10.1016/j.ijheatmasstransfer.2020.120633.
17. Bejan A, Errera MR. Convective trees of fluid channels for volumetric cooling. Int J Heat Mass Transf. 2000;43(17):3105–18. doi:10.1016/S0017-9310(99)00353-1.
18. Bejan A. Constructal tree-shaped paths for conduction and convection. Int J Energy Res. 2003;27(4):283–99. doi:10.1002/er.875.
19. Bendsøe MP, Kikuchi N. Generating optimal topologies in structural design using a homogenization method. Comput Methods Appl Mech Eng. 1988;71(2):197–224. doi:10.1016/0045-7825(88)90086-2.
20. Borrvall T, Petersson J. Topology optimization of fluids in Stokes flow. Numer Methods Fluids. 2003;41(1):77–107. doi:10.1002/fld.426.
21. Zhao Q, Zhang H, Wang F, Zhang T, Li X. Topology optimization of non-Fourier heat conduction problems considering global thermal dissipation energy minimization. Struct Multidiscip Optim. 2021;64(3):1385–99. doi:10.1007/s00158-021-02924-0.
22. Koga AA, Lopes ECC, Villa Nova HF, de Lima CR, Silva ECN. Development of heat sink device by using topology optimization. Int J Heat Mass Transf. 2013;64(3):759–72. doi:10.1016/j.ijheatmasstransfer.2013.05.007.
23. Palumbo J, Tayyara O, Amon CH, Chandra S. Topologically optimized mini-channel heat sinks for reduced temperature non-uniformity. Int J Heat Mass Transf. 2023;214:124421. doi:10.1016/j.ijheatmasstransfer.2023.124421.
24. Vafai K, Zhu L. Analysis of two-layered micro-channel heat sink concept in electronic cooling. Int J Heat Mass Transf. 1999;42(12):2287–97. doi:10.1016/S0017-9310(98)00017-9.
25. Tang XP, Liu HL, Wei LS, Tang CG, Shao XD, Shen H, et al. Numerical investigation and experimental verification of topological optimized double-layer mini-channels. Int J Heat Mass Transf. 2023;215(5):124513. doi:10.1016/j.ijheatmasstransfer.2023.124513.
26. Lazarov BS, Sigmund O. Filters in topology optimization based on Helmholtz-type differential equations. Numer Methods Eng. 2011;86(6):765–81. doi:10.1002/nme.3072.
27. Wang F, Lazarov BS, Sigmund O. On projection methods, convergence and robust formulations in topology optimization. Struct Multidiscip Optim. 2011;43(6):767–84. doi:10.1007/s00158-010-0602-y.
28. Liu Y, Chen C, Yuan Y, Yang J, Guo Z, Shi J. Study of microchannel heat transfer characteristics based on topology optimization. Int J Therm Sci. 2025;214(2):109898. doi:10.1016/j.ijthermalsci.2025.109898.
29. Svanberg K. A class of globally convergent optimization methods based on conservative convex separable approximations. SIAM J Optim. 2002;12(2):555–73. doi:10.1137/s1052623499362822.
30. Zeng S, Liu J, Ma C. Topology optimization in cooling moving heat sources for enhanced precision of machine tool feed drive systems. Int J Therm Sci. 2024;202(7):109065. doi:10.1016/j.ijthermalsci.2024.109065.
31. Wang D, Song H, Wang G, Yang Y, Wang S, Xiang S. Optimal arrangements of inlet and outlet in topology liquid-cooled microchannel heat sink based on multi-objective optimization. Int J Therm Sci. 2025;209(1):109552. doi:10.1016/j.ijthermalsci.2024.109552.
32. Zhou J, Lu M, Zhao Q, Hu D, Qin H, Chen X. Thermal design of microchannel heat sinks using a contour extraction based on topology optimization (CEBTO) method. Int J Heat Mass Transf. 2022;189(6):122703. doi:10.1016/j.ijheatmasstransfer.2022.122703.
33. Qian S, Lou S, Ge C, Wang W, Tian X, Cai Y. The influence of temperature dependent fluid properties on topology optimization of conjugate heat transfer. Int J Therm Sci. 2022;173(1):107424. doi:10.1016/j.ijthermalsci.2021.107424.
34. Popiel CO, Wojtkowiak J. Simple formulas for thermophysical properties of liquid water for heat transfer calculations (from 0°C to 150°C). Heat Transf Eng. 1998;19(3):87–101. doi:10.1080/01457639808939929.

35. Mo X, Zhi H, Xiao Y, Hua H, He L. Topology optimization of cooling plates for battery thermal management. Int J Heat Mass Transf. 2021;178:121612. doi:10.1016/j.ijheatmasstransfer.2021.121612.
36. Chen X, Wang X. Microchannel cold plate heat transfer and flow resistance characteristics calculation and structure optimization. J Phys Conf Ser. 2020;1676(1):012204. doi:10.1088/1742-6596/1676/1/012204.
37. Tan H, Wu L, Wang M, Yang Z, Du P. Heat transfer improvement in microchannel heat sink by topology design and optimization for high heat flux chip cooling. Int J Heat Mass Transf. 2019;129(5):681–9. doi:10.1016/j.ijheatmasstransfer.2018.09.092.
38. Ali N, Haque I, Alam T, Siddiqui TU, Ahmad Ansari M, Yadav J, et al. Numerical investigation on heat transfer and flow mechanism in microchannel heat sink having V shape ribs. Case Stud Therm Eng. 2025;65:105684. doi:10.1016/j.csite.2024.105684.
39. Shen H, Wang CC, Xie G. A parametric study on thermal performance of microchannel heat sinks with internally vertical bifurcations in laminar liquid flow. Int J Heat Mass Transf. 2018;117:487–97. doi:10.1016/j.ijheatmasstransfer.2017.10.025.
40. Qin Y, Li L, Zhao Y, Chen Z, Wang X, Xu B. Experimental and numerical investigation of liquid-cooled microchannel heat sink by topology optimization for uniform heat source. Int J Heat Mass Transf. 2026;256(1):127932. doi:10.1016/j.ijheatmasstransfer.2025.127932.